RSC Advances

ROYAL SOCIETY OF CHEMISTRY

www.rsc.org/advances

RSC Advances

RSCPublishing

ARTICLE

Cite this: DOI: 10.1039/xoxxooooox

Received ooth January 2012,
Accepted ooth January 2012

DOI: 10.1039/xoxxooooox

www.rsc.org/

Vibrational study of adsorption of Congo red onto TiO_2 and the LSPR effect on its photocatalytic degradation process

M. L. de Souza,[a] D. C. Tristão[a] and P. Corio[a] ,

Chemical interaction between the azo dye Congo Red (CR) and two photocatalysts based on titanium dioxide (commercial Degussa P25 TiO_2 and nanostructured TiO_2, primarily in the form of anatase) were analyzed by diffuse reflectance and resonance Raman spectroscopies. The adsorption isotherms of the dye over the photocatalysts were consistent with Langmuir adsorption model. High similarity between the CR dye adsorbed onto P25 TiO_2 and the product of CR oxidation/acidification (hydrazone tautomer) was observed through resonance Raman spectroscopy. The vibrational results were consistent with the analysis of the Langmuir isotherm, where chemisorption of CR on P25 and physisorption of CR on nanoTiO_2 were in accordance with the obtained K_{ads} and q_{max}. The addition of plasmonic Ag NPs was performed in order to analyze effects on TiO_2 photocatalytic efficiency. The CR photodegradation with the plasmonic catalyst presented an increase on k_{obs} of 14 % and 100 % to P25 and nanoTiO_2, respectively. The catalysis improvement was assigned to the near field enhancement due to the Ag NPs plasmonic effect.

Introduction

Advanced Oxidative Processes (AOPs) have been used as viable alternatives for the treatment of effluents contaminated by organic compounds due to their high efficiency compared to physical and biological processes. AOPs degrade contaminants and may result in their mineralization, in contrast to physical processes, such as the use of charcoal, which result in the transfer of contaminants to different sites. With regard to biological processes, these are limited by the capacity of the microorganisms to degrade certain chemical species.

Among the AOP is the heterogeneous photocatalysis, which is mediated by a semiconductor catalyst. The most commonly employed semiconductor material is titanium dioxide (TiO_2) due to its favourable characteristics, such as low cost, low toxicity and high efficiency. The main polymorphs of TiO_2 are anatase, rutile and brookite. Commercial Degussa P25 TiO_2 (P25), consisting of 25% rutile and 75% anatase phases, has been employed as a standard catalyst in heterogeneous photocatalysis. Although the energy gap between the valence band and the conduction band (band gap energy, E_{gap}) of P25 is approximately 3.20 eV (for pure anatase E_{gap} = 3.20 eV and for pure rutile E_{gap} = 3.00 eV), studies have suggested that the high catalytic efficiency of this material is due to the synergistic effect between its constituent phases. [1]

Therefore, during the photoexcitation an electron is promoted from the valence to the conduction band generating a vacancy on the valence band (the so-called electron/hole pair) in TiO_2 requiring energy in the ultraviolet region. This represents a significant limitation to the employment of TiO_2 in photoconversion systems based on sunlight, since the UV radiation represents less than 5% of solar radiation while visible radiation accounts for approximately 45%. Current research in the area of photocatalysis has focused on the development of catalyst materials with higher activity and efficiency. [2-5]

Localized Surface Plasmon Resonance (LSPR) occurs in nanoscale (10-200 nm) particles of noble metals that absorb and scatter (and amplify) electromagnetic radiation through collective oscillations of valence electrons. The effectiveness of these nanoparticles is dependent on the metal used as well as on the shape, size and dielectric constant of the particles and of their surroundings. [8] The addition of metal nanoparticles capable of sustaining LSPR to interact with the semiconductor catalyst has been considered to be a very promising approach to amplify the radiation in the UV/visible edge region of TiO_2 absorption/excitation. [6,7]

Moreover, the study of the physical and chemical properties of the interaction between an analyte and the solid catalyst is essential to understand interfacial processes in order to propose degradation mechanisms or obtain detailed information

regarding the catalysis byproducts. In this context, Raman spectroscopy is an advantageous technique for the verification of structural changes associated with adsorption processes.

The photocatalytic degradation of a dye in aqueous media is a well-established method for evaluating the TiO_2 photocatalysis efficiency in the absence and in the presence of plasmonic structures. The dye Congo red (CR) is an azo compound first synthesized in Germany in 1883 during an intense search for textile dyes with the ability to react with fibers (direct dyes) and maintain resistance to discoloration. [9] Since 1922, CR has been widely used in bioanalytical staining procedures in the study and diagnosis of amyloidosis and neurodegenerative diseases such as Alzheimer's. Highly carcinogenic byproducts, however, are formed during its metabolization or decomposition by degradation processes. Although CR is not currently employed as a textile dye, azo compounds are of great interest in the study of photocatalytic processes because they are widely employed in the textile industry and extensively used in analytical chemistry as acid-base, redox and metallochromic indicators.

The interaction of CR with the surface of two TiO_2-based photocatalysts (P25 and a nanostructured material prepared in laboratory consisting mostly of the anatase phase) was studied employing Raman spectroscopy to elucidate the structural changes arising from chemisorption processes and to correlate the surface interactions with the efficiency of the photodegradation process. The vibrational study of interfacial processes may be helpful in verifying the LSPR effect in the photocatalytic process. Silver was chosen as the noble metal for use in this study due to the congruence between its LSPR extinction and the low edge excitation wavelength of the TiO_2, facilitating the verification of the plasmon effect on the photocatalytic process.

Experimental

2.1. Materials and instrumentation

Commercial Degussa P25 TiO_2 Aeroxide® (P25) with surface area of 50 m^2 g^{-1} and mean particle size of 21 nm was employed as the standard catalyst and purchased from Degussa-Evonik. CR - Direct Red 28-22120 (Figure 1), ethylene glycol (EG), silver nitrate ($AgNO_3$), tris(acetylacetonate) iron (III) ($Fe(acac)_3$), sodium bromide (NaBr), polyvinylpyrrolidone 55000 (PVP), titanium (IV) isopropoxide and glacial acetic acid (all analytical grade) were purchased from Sigma-Aldrich and used without further purification. The aqueous solutions were prepared using double-distilled water.

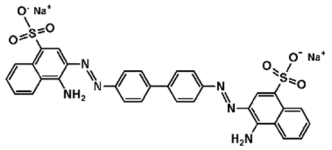

Figure 1. Structural formula of CR (sodium 3,3′-[(1,1′-biphenyl)-4,4′-diyl(azo)]bis(4-aminonaphtalenesulfonate), CAS 573-58-0).

Diffuse Reflectance (DR) and UV-VIS-NIR spectra were obtained with a Shimadzu UVPC-3101 scanning spectrophotometer. Raman spectra were acquired with a Renishaw InVia Reflex spectrometer coupled to a Leica DM 2500M microscope, 632.8 nm He/Ne and 785.0 nm diode laser excitation and a CCD detector with a spatial resolution of approximately 1 μm^2 (micro-Raman technique). The experiments were performed using a back-scattering geometry and the laser beam was focused on the sample by a ×100 lens. FT-Raman spectra of solid samples were recorded with an RFS 100 FT-Raman Bruker spectrometer using 1064.0 nm radiation from a Nd:YAG laser. Pore diameter was determined according to the BET method, using a Quantachrome NOVA 1200e instrument. Powder X-ray diffraction (XRD) was performed on a Rigaku Miniflex diffractometer, with Cu Kα radiation (λ= 0.15406 nm).

2.2. Nanostructured TiO_2 and Ag NPs synthesis

The nanostructured TiO_2 photocatalyst (nanoTiO_2) was obtained according to the procedure proposed by Murugesan et al. [10] through acid hydrolysis of an organic precursor. The silver nanowires (Ag NPs) were synthesized following the protocol proposed by Xia et al. [11]

2.3. Experimental procedures for adsorption and photodegradation processes

The photodegradation process was performed in a reactor consisting of a 125 W Philips HPL-N Hg lamp without the glass bulb (irradiance of ca. 108 W m^{-2} for $\lambda > 254$ nm) as the radiation source placed 20 cm immediately above a borosilicate cylindrical cell with lateral input/output of water for thermal conditioning (20 ± 0.1 °C), an open-to-air top and 6 cm diameter.

The suspensions degraded consisted of 100 mL of a 20 mg L^{-1} CR aqueous solution containing 0.5 g L^{-1} of photocatalyst (either P25 or nanoTiO_2) in the presence and absence of approximately 1% Ag NPs. Adsorption isotherms were obtained in the same system, but without the radiation source and in a wider concentration range (from 5 to 30 mg L^{-1}). Aliquots of 2 mL were withdrawn periodically during the adsorption/degradation processes and centrifuged twice at 13,400 rpm to remove the supernatant. The degraded solution temperature was monitored by a thermostat connected to an external multimeter.

CR adsorption isotherms for both catalysts in the absence and presence of Ag NPs were built using the supernatant maximum absorption band in the visible region in aqueous solution (498 nm). The degradation process was studied based on the solution bleaching under UV/visible irradiation (relative decrease in the 498 nm absorption band) as a function of the irradiation time and the solution pH was monitored. The solids resulting from adsorption isotherm and photodegradation experiments were analysed by Raman spectroscopy.

Results and discussion

3.1. Physicochemical properties of the photocatalysts

The Raman spectra obtained with laser excitations at 632.8 nm and 1064 nm, and the XRD patterns of the photocatalysts are shown in Figure 2. The Raman spectra for nanoTiO_2 obtained at both laser excitations suggest that this photocatalyst is comprised mainly of the anatase phase due to the presence of the bands at 143, 396, 515 and 638 cm^{-1} in agreement with the anatase signature XRD diffractogram peak at 25°. The nanoTiO_2 synthesized had an average particle diameter of 16 nm (determined using the Scherrer equation). The Raman spectrum for P25 obtained at an excitation of 1064 nm showed no notable differences in relation to the nanoTiO_2 spectrum, however the Raman spectrum obtained at an excitation of 632.8 nm presented, beside the anatase bands, a band associated with rutile at 445 cm^{-1} and a shoulder at 610 cm^{-1} overlapped with the band at 637 cm^{-1} causing its broadening. The XRD pattern verified the P25 composition, showing anatase and rutile signature peaks at 25° and 27°, respectively. [12,13] Thus, the two techniques provide consistent results regarding the crystallinity and composition of the catalysts.

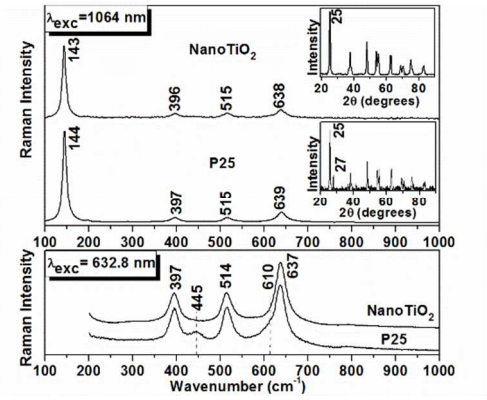

Figure 2. Raman spectra of P25 and nanoTiO_2 obtained with laser excitation of 1064 nm and 632.8 nm (respective XRD patterns shown in the inset).

Of the three crystalline phases of TiO_2, it is reported that the photocatalytic activity of the anatase phase is greater compared with the brookite and rutile pure phases but lower compared with P25. [1] With the use of a photocatalyst comprised mainly of the anatase phase (lower catalytic activity compared to P25) the plasmonic effect on the photocatalytic degradation of a proof-of-concept molecule can be clearly observed.

According to the BET data (Figure 3 (A)) the P25 presented average surface area of 45 m^2 g^{-1}, average pore radius of 1.8 nm and pore volume of 0.114 cc g^{-1}. The adsorption/desorption profiles were similar and indicated a cylindrical pore morphology. The nanoTiO_2 (Figure 3 (B)) presented a surface area of 80 m^2 g^{-1}, average pore radius of 5.2 nm and pore volume of 0.188 cc g^{-1}. The desorption process for this material was less efficient than the adsorption process, which is characteristic of pores with narrow orifices and wide interiors.

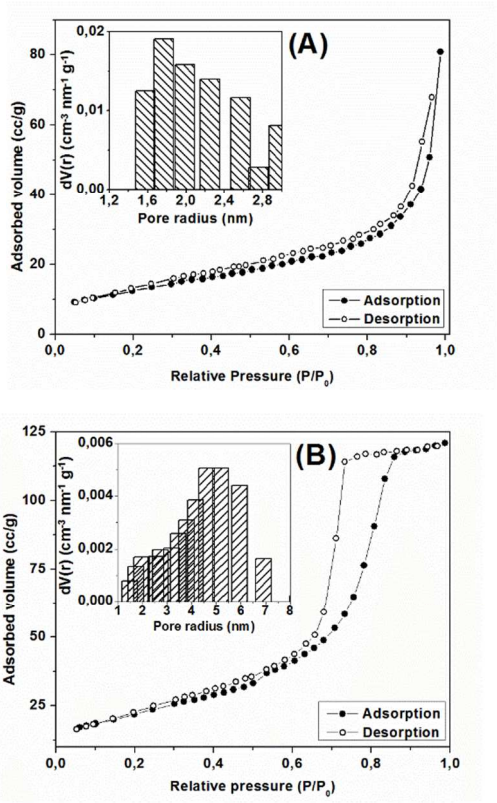

Figure 3. BET isotherm adsorption/desorption analysis and pore volume insets (A) P25 and (B) nanoTiO_2.

Beside the catalytic efficiency of the semiconductors, the BET isotherms revealed that nanoTiO_2 would provide greater contact surface with the analyte compared to P25, however the pore structures would block the movement of molecules and byproducts and thus cause a decrease in the efficiency of the material.

3.2. CR adsorption isotherms for the catalysts

The CR adsorption isotherms for the catalysts were obtained at 20 ± 0.1 °C with dye concentrations ranging from 5 to 30 mg L^{-1}. The adsorption/desorption equilibrium for all concentrations was achieved after approximately 1 h, with stirring in the dark, and was monitored by UV-VIS spectroscopy. The profiles obtained for the systems investigated were consistent with the Langmuir adsorption model, with correlation coefficients higher than 0.99. Table 1 shows the data obtained for the adsorption of CR onto the catalysts.

Table 1. Langmuir isotherm parameters for the adsorption of CR onto the catalysts and catalyst/ Ag NPs mixtures.

Catalytic system	R^2	K_{ads} L µmol^{-1}	q_{max} µmol g^{-1}	n_{ads} µmol m^{-2}
CR + P25	0.999	4.11	45.5	1.82
CR + P25 + Ag NPs	0.997	9.67	33.9	1.36
CR + nanoTiO_2	0.997	5.08	23.4	0.272
CR + nanoTiO_2 + Ag NPs	0.991	1.32	23.7	0.276

K_{ads} is adsorption equilibrium constant; q_{max} is maximum amount of dye adsorbed per catalyst mass; n_{ads} is number of mols of dye adsorbed per catalyst area.

For the system containing only the Ag NPs, it was not possible to remove the solid by centrifugation due to the low amount of Ag NPs and the adsorption isotherm for this system could not be obtained. Therefore, due to the low amount of Ag NPs, CR removal from the solution through adsorption was assumed not to be significant in this system.

The q_{max} for P25 was around two times greater than the corresponding value for nanoTiO_2, even though the surface area of the latter is around two times larger. The difference between the n_{ads} values for the catalysts was even greater (1.82 for P25 and 0.272 for nanoTiO_2). The distinct surface chemistry properties of each catalyst can address the given result considering the different synthesis procedures for each material and which can strongly influence the interaction between the dye and the catalyst. Also the affinity to a specific polymorph present only in P25, rutile for instance, must be considered.

The Ag NPs are stabilized by PVP and have distinct effects on the different catalysts under CR adsorption. The interaction between the PVP and TiO_2 [14] caused changes in the availability and strength of the adsorption sites onto both catalysts. The presence of Ag NPs on P25 resulted in a 25% lower q_{max} value compared to bare P25, and the slight effect on the q_{max} value for the nanoTiO_2. This result suggests that the Ag NPs protected by PVP interact strongly with the rutile phase in agreement with the estimated portion of rutile in P25. The interaction between Ag NPs and TiO_2 hinders the adsorption of CR onto P25 by decreasing the number of adsorption sites available, while it has no effect in the amount of CR adsorbed onto nanoTiO_2.

Although there is a decrease in the availability of adsorption sites on P25 due to the presence of Ag NPs, the CR adsorption equilibrium constant (K_{ads}) on P25+Ag NPs was favoured by reaching the equilibrium faster than in bare P25. In addition, there was a lower K_{ads} to CR+nanoTiO_2+Ag NPs than to CR+nanoTiO_2. These results indicated that the interaction between CR and the Ag NPs exerts a competition with TiO_2 stronger in nanoTiO_2 than in P25, which might be associated to the surface chemistry of the photocatalysts.

The higher value of q_{max} to the CR+P25 (25 %) and the slight changes on q_{max} to the CR+nanoTiO_2 system, both related to the systems after adding Ag NPs, suggest a strong interaction between CR and anatase phase and between the Ag NPs and rutile phase.

3.3. Adsorption of CR onto the catalyst materials investigated through electronic and vibrational spectroscopies

On investigating the effect of the surface processes on the catalysis, the chemisorption and physisorption processes need to be considered since they can affect the mechanisms involved in heterogeneous photocatalysis. The adsorption pathway was observed by way of the electronic and vibrational spectra through the interaction between CR and the semiconducting catalysts, aiming to relate these findings to the results obtained with the adsorption isotherm parameters of the CR catalysts.

CR was found to act as a local pH indicator at the surface depending on the catalyst, since it is a pH indicator in the range of 3.0 to 5.2, changing colour from red to violet in alkali medium. [15] The UV-VIS spectrum of the CR aqueous solution is presented in Figure 4 (A) and the CR interactions with the catalysts were investigated through the DR spectra presented in Figure 4 (B).

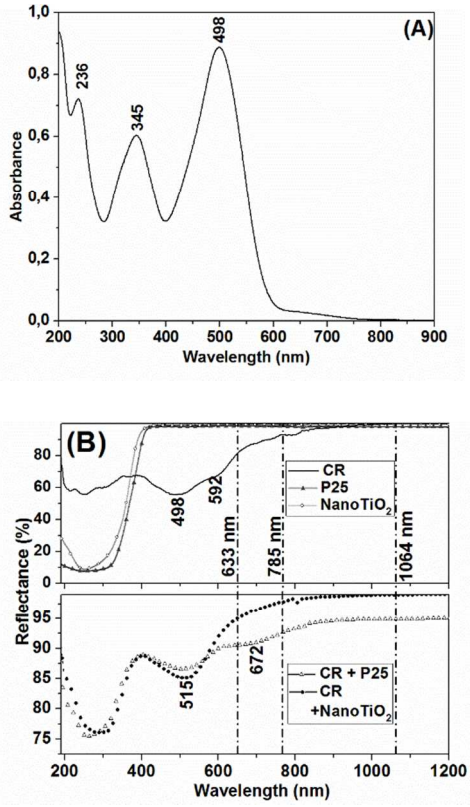

Figure 4. (A) UV-VIS spectrum of CR in aqueous solution 2.0 × 10^{-5} mol L^{-1}; (B) DR spectra of the pure photocatalysts, pure CR and CR+photocatalysts in KBr tablets (vertical dashed lines indicate the excitation wavelengths of the Raman spectroscopy analysis).

The maximum peak in Figure 4 (A) at 498 nm also corresponds roughly to the peak maximum for the CR solid in $BaSO_4$ in Figure 4(B), although the solid spectrum has a shoulder at 592 nm due to intermolecular interactions. The DR spectrum for the CR+P25 and CR+nanoTiO_2 showed in Figure 4 (B) presents a 15 nm red-shift in the maximum peak band to 515 nm. Considering the pH indicator behaviour of CR, the

band that arises at approximately 670 nm on the CR+P25 spectrum suggests the acid/base interaction of CR with the P25 surface (turning violet coloured), while in the case of CR+nanoTiO$_2$ there was not enough evidence to suggest an interaction pathway.

The energy of the excitation line at 785 nm is in resonance with the electronic transition observed in the DR spectrum of CR+P25 (absorbance band at 672 nm in Figure 4(B)) regarding the interaction between CR and P25, and therefore should enhance the Raman modes related to this electronic transition – resonance Raman (RR) effect. On the other hand, the CR+nanoTiO$_2$ system at both 785 and 1064 nm, along with the CR+P25 at the 1064 nm excitation line, did not present RR and so present ordinary Raman scattering.

Figures 5 (A) and (B) show the Raman spectra of CR adsorbed onto the two photocatalysts (P25 and nanoTiO$_2$) in the absence and presence of Ag NPs, with excitations at 785 nm (RR for CR+P25) and 1064 nm.

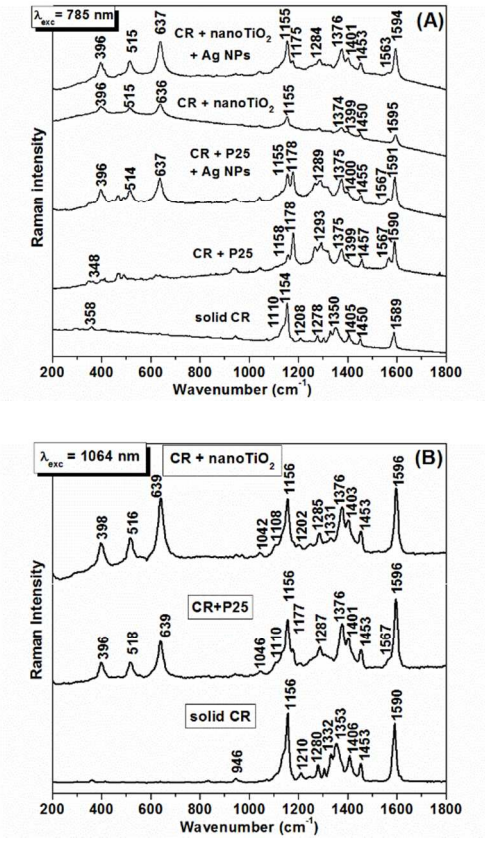

Figure 5. Raman spectra of solid CR and CR adsorbed onto P25 and onto nanoTiO$_2$, in the absence and in the presence of Ag NPs. (A) λ_{exc} = 785 nm and (B) λ_{exc} = 1064 nm. All samples were obtained from the catalyst adsorption system initially containing 20 mg L^{-1} CR and 0.5 g L^{-1} photocatalyst after 180 min stirring in the dark.

The vibrational assignments to the main CR bands and CR+P25 are presented in Table 2.

Table 2. Assignment of Raman bands of CR and CR adsorbed on P25.

Wavenumber / cm^{-1}				
Solid CR	***CR+P25***		*Assignments*	*Ref.*
λ_{exc} *(nm)*	λ_{exc} *(nm)*			
785	*785*	*1064*		
1110	-	1110	ν_s (SO_3^-)	15
1154	1158	1156	ν (C–N=)	16, 17
-	1178	-	ν (N–N)	16
1208	-	1208	ν_{as} (SO_3^-)	15
-	1267	-	ν (C–N–)*	15, 16, 18
1278	-	-	ν(C–N=), δ(C–H)	19
-	1293	1287	ν (C–N–)*	16
-	1315	-	δ(C–H)* ν(C–NH_2)	19
1330	-	-	δ (C–H) azo	19
1350	-	-	ν (C=C) naphthyl	17, 18
-	1375	1376	ν (N=N)	16, 18
1405	1399	1401	ν (N=N)	16, 17
1450	1457	1453	ν (C=C) aromatic ring	15, 16, 18
-	1567	1567	ν (C=N–)*	15, 16
1589	1590	1596	ν (C–C) aromatic ring	15-18

ν – stretching; as – asymmetric; s – symmetric; δ – bending.* hydrazone tautomer.

In Figures 5(A) and (B), the bands at 396, 515 and 637 cm^{-1} are assigned to TiO_2. Significant changes are observed in the RR spectra of CR adsorbed onto P25 (Figure 5 (A)), including the relative decrease of the TiO_2 bands due to the RR effect of the dye and the appearance of bands at 1178 cm^{-1} related to the asymmetric stretching of the (N–N) groups and 1567 cm^{-1} related to (ν C=N–) from the emerging hydrazone structure (Table 2). The intensity of the bands at 1154 cm^{-1} (ν C–N=) and at 1405 cm^{-1} (ν N=N) decrease and the appearance of bands centred at 1293 cm^{-1} (hydrazone ν C–N–) in relation to the biphenyl group, which was also observed on the spectra for CR adsorbed onto P25 in the presence of Ag NPs, indicate the formation of the azo-hydrazone tautomer. Li and Diebold [21] showed that the adsorption of azobenzene to TiO_2 anatase and rutile happens through the azo moiety causing cleavage under high coverage with few undissociated molecules, and without dissociation under low coverage, supporting the present Raman results.

The system containing CR adsorbed onto nanoTiO$_2$ in Figure 5 (A) differs from the solid CR only with regard to the band positioned at 1405 cm^{-1} (ν N=N) shifted to 1400 cm^{-1}, the disappearance of the band at 1350 cm^{-1} (ν C=C naphtyl) and the enhancement of the band at 1375 cm^{-1} (ν N=N). The disappearance of the band at 1207 cm^{-1} (ν_{as} SO_3^-) was observed for CR adsorption on both semiconductors under the 785 nm excitation laser, however it appears with small shift under the 1064 nm excitation laser. The system containing CR+nanoTiO$_2$ and Ag NPs under the 785 nm excitation laser shows the same

bands observed for the CR+nanoTiO$_2$ but with an increase in intensity. Once again, the intensification of these bands is associated with the presence of LSPR in the Ag NPs due to the field intensification and increase in the intensity of the Raman scattering.

Bonancêa et al. reported results for the Raman spectra of CR after chemical oxidation, electrochemical oxidation and at pH 1. [18] Molecules with an azo moiety may form a hydrazone group through the reduction of the N=N bond or insertion of an H^+ ion. Based on the spectra obtained and the vibration assignments presented in Table 2, the adsorption of CR onto P25 results in an analogous byproduct and involves the formation a C=N-NH group and influence on the mode related to the sulfonate group on the Raman spectra (observed only on excitation at 1064 nm).

Considering the different excitation energies used to obtain the spectra of Figures 5 (A) and (B), it is possible to propose that the bands observed in the RR (Figure 5 (A)) overlap the bands observed in the ordinary Raman visible in Figure 5 (B). Interesting changes are also observed in the FT-Raman spectra (Figure 5 (B)) when we compare the spectra for the solid CR with that for the dye adsorbed onto the photocatalysts. In the latter case there is the appearance of bands at 1110 cm^{-1}, the disappearance of the band at 1332 cm^{-1} and a shift in the bands at 1278, 1350 and 1589 cm^{-1} to 1287, 1376 and 1596 cm^{-1}, respectively, compared to the solid CR under the same excitation laser.

Figure 6 shows the Raman spectrum for the solid CR, CR adsorbed onto P25 and nanoTiO$_2$, acidic and chemically oxidized CR.

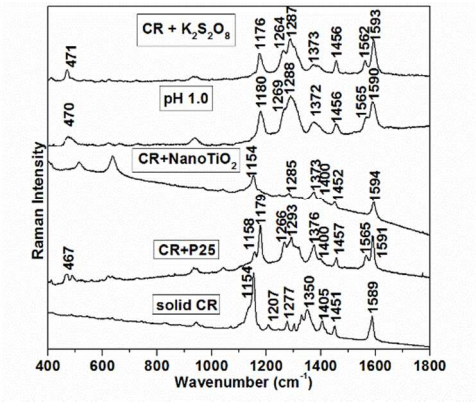

Figure 6. Raman spectra for solid CR, CR+P25, CR+NanoTiO$_2$, CR chemically oxidized by $K_2S_2O_8$ (λ_{exc} = 785 nm) and acidic CR at pH 1.0 (λ_{exc} = 632.8 nm).

The spectra for the solid CR, CR adsorbed onto P25 and onto nanoTiO$_2$ and chemically oxidized CR were obtained at an excitation of 785 nm because the Raman signal of the dye is more intense at this radiation wavelength than when excited at 632.8 nm, where the strong fluorescence background hinders the observation of the characteristic CR vibrational modes. There is a clear similarity between the spectra for the CR at pH 1.0, chemically oxidized and adsorbed onto P25. According to Table 2, the bands which appear in the region of 1287 cm^{-1} and 1562 cm^{-1} are related to the hydrazone tautomer, which is sensitive to the pH and similar to the oxidation process, [18] as observed to the spectrum for CR adsorbed onto P25. These data suggest that chemisorption of the azo dye onto P25 occurs and that this process resembles the oxidation/acidification process.

On the other hand, there are few differences between the spectra for the CR solid and the CR adsorbed onto nanoTiO$_2$ in Figure 5(A). The persistence of the bands at 1400 cm^{-1} and 1450 cm^{-1} and the disappearance of the band at 1350 cm^{-1} (naphthyl) and enhancement of the band at 1373 cm^{-1} suggest that there is no change in the azo moiety and that the interaction between the CR and nanoTiO$_2$ occurs without formation of hydrazone tautomer. The disappearance of the ν_{as} SO_3^- at 1207 cm^{-1} under 785 nm excitation agrees with the previous reports which suggested that sulfonated dyes are favorable to chemisorption on TiO$_2$ through the SO_3^- groups [15,17], on the other hand, under 1064 nm excitation laser (out of resonance) physisorbed CR molecules are evidenced.

Therefore, through the use of Raman spectroscopy to identify the mechanism involved in the adsorption of CR onto P25 and onto nanoTiO$_2$, it is concluded that the strong interaction with P25 indicated by the Langmuir isotherm is associated with an adsorption mechanism involving chemisorption forming the structure-like azo-hydrazone tautomer. In the systems where the interaction was not as strong according to the Langmuir isotherm (nanoTiO$_2$), physisorption through the SO_3^-/naphthyl moiety was observed.

3.4. Photocatalytic Degradation

Figures 7 (A) and (B) show CR degradation catalyzed by P25 and nanoTiO$_2$ under UV/visible irradiation. It was observed that the process of direct photolysis occurs through UV/visible irradiation (Hg lamp emission lines). Even though this process does not produce maximum degradation even after 240 min of exposure, the process of photolysis should be considered in the analysis of the photocatalytic results. The degradation catalyzed by P25 (Figure 7 (A)) showed higher efficiency than that catalyzed by nanoTiO$_2$ (Figure 7 (B)), thus confirming the synergism between the anatase and rutile phases.

The results shown in Figures 7 (A) and (B) revealed interesting trends. The Ag NPs did not exhibit catalytic activity in the absence of the semiconductor, as compared to the photolysis. However, P25 or nanoTiO$_2$ catalysis in the presence of the Ag NPs caused an increase in the apparent kinetic constant (k_{obs}) of photodegradation. The k_{obs} of the semiconductor+Ag NPs mixture was normalized by the k_{obs} of the respective semiconductor yielding a $k_{ratio} > 1$ when there is an improvement in the efficiency. The values for the k_{ratio} for the CR degradation catalyzed by P25 and nanoTiO$_2$ were 1.14 and 2.00, respectively. These results verified the beneficial effect of the addition of Ag NPs and, since the Ag NPs had no catalytic effect and the Ag NPs are involved by a thick organic layer (PVP) which prevents charge transfer, the phenomenon responsible for the improvement in the catalytic efficiency may

be associated with the near field intensification by the LSPR at the semiconductor surface which improves the electron-hole events. [7,22]

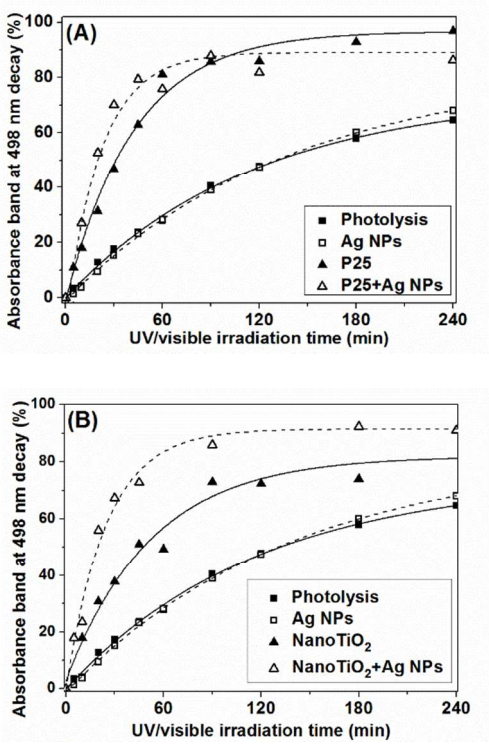

Figure 7. CR absorbance band decay at 498 nm as a function of irradiation time catalysed by (A) P25 and (B) nanoTiO$_2$; in the presence and absence of Ag NPs.

The maximum degradation shown on the degradation profile in the presence of Ag NPs was between 80 and 90 % for both systems, possibly due to the desorption of the Ag NPs from the catalysts through degradation processes of the PVP. For instance, the system containing P25 and Ag NPs (Figure 7 (A)) demonstrated an improvement in the kinetics of the catalytic effect of P25 due to the presence of Ag NPs, with maximum degradation being achieved in 60 min. However, a maximum degradation of 80% was achieved in the presence of Ag NPs while 90% degradation was observed with only P25 as the catalyst. It should be noted that the nanoTiO$_2$ had a lower catalytic effect than P25, as expected. However, the addition of Ag NPs allowed this catalyst to achieve the same degradation amount of CR catalysed by P25 (approximately 85 %).

As discussed in Sections 3.2 and 3.3, the amount of CR adsorbed onto nanoTiO$_2$ was lower than in the case of P25 and the interaction between the dye and nanoTiO$_2$ was assumed to occur through physisorption, while for P25 a chemisorption process was assumed to occur. These results suggest that the degradation mechanism in each system is distinct, although the Ag NPs exert the same influence on both semiconductor material.

The Raman spectra of the catalysts after 300 min degradation are shown in Figure 8. The degradation of CR catalysed by P25 presented similar RR spectrum to its adsorption spectrum in Figure 5(A), however there was an increase in relative intensity of the TiO$_2$ bands under these conditions due to the consumption of CR and its hydrazone tautomer. On the other hand, after 300 minutes of UV/visible irradiation, the spectrum of the P25+Ag NPs catalysis presented a decrease of the bands at 1154 and 1400 cm^{-1} assigned to the azo moiety while the vibrational modes of the hydrazone tautomer remained and the TiO$_2$ bands were not evidenced due to the RR effect of the hydrazone tautomer.

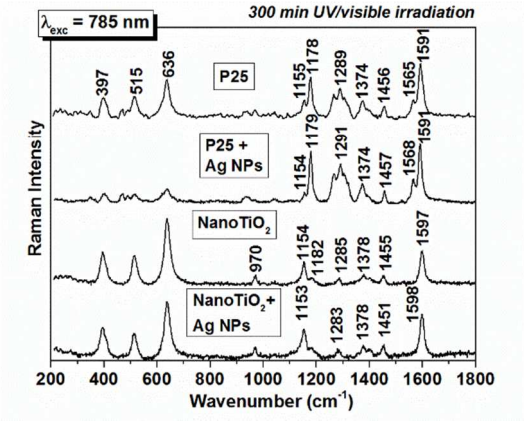

Figure 8. Raman spectra of CR adsorbed onto the catalysts after 300 minutes UV/visible irradiation.

The nanoTiO$_2$ and nanoTiO$_2$+Ag NPs Raman spectra containing CR after 300 minutes degradation presented no significant changes in the vibrational region of CR compared to the adsorbed CR spectra but the emergence of band at 970 cm^{-1}. This band is also present in the chemically oxidized and acidic products in Figure 6.

The analysis of the catalyst surfaces by Raman spectroscopy suggests that the degradation products do not remain adsorbed to the catalyst surfaces, as revealed by the similarities between the spectra obtained after adsorption and after degradation. In addition, the photodegradation mechanism was shown to be distinct to each catalyst. For instance the catalysis employing P25+Ag NPs favours the consumption of the azo groups over the hydrazone groups while P25 causes the similar consumption of both structures, evidenced by the relative intensity of the bands at 1154 cm^{-1} and 1178 cm^{-1}. The 1154 cm^{-1}/1178 cm^{-1} intensity ratio (azo peak/hydrazone peak) to P25+Ag NPs after adsorption was 0,86 and after degradation was 0,19 revealing the consumption of the azo species and to P25 it was reached 0,28 and 0,39 respectively indicating not significant changes in the azo/hydrazone proportion. A possible explanation to this behaviour is related to changes in the solution pH during degradation, which influences the surface equilibrium of the adsorbed tautomeric species. Considering the improvement of the kinetic parameter of P25+Ag NPs compared to bare P25, the increased H$^+$ formed in this case favours the azo-hydrazone tautomer.

Conclusions

The isotherm parameters indicated a stronger interaction between CR and P25 than between CR and nanoTiO_2 corroborated by the appearance of a band at 672 nm, which allowed the resonance Raman investigation of the adsorption processes. Resonance Raman spectroscopy under 785 nm indicated that the interaction between CR and P25 occurs through a process similar to the oxidation/acidification of CR in aqueous solution (azo-hydrazone tautomer), and this was not observed when CR was adsorbed on nanoTiO_2, nor under 1064 nm. The investigation of the adsorption process of CR onto two different TiO_2-based catalysts employing Resonance Raman spectroscopy was successfully performed and elucidated the physisorption and chemisorption by the formation of the hydrazone tautomer. The comparisons with the oxidation/acidification products were important to propose an adsorption mechanism.

The Raman analysis of the degraded suspension after 300 min irradiation evidenced that the presence of Ag NPs along P25 favours the consumption of the azo structures on the catalyst surface while its absence causes the degradation and consumption of both CR and hydrazone tautomer, as observed to bare P25 and to nanoTiO_2 catalytic systems. The investigation of the adsorption process of the dye onto de catalyst was fundamental to the understanding of the implications of the Ag NPs over the catalysts in order to avoid confusion in determining the degradation byproducts.

The addition of Ag NPs to both catalytic systems resulted in an improvement in the apparent kinetics constant (k_{obs}); however, the catalysis stopped when approximately 90 % degradation was reached. The catalytic improvement due the addition of Ag NPs was attributed to the near field intensification at the semiconductor surface through LSPR.

Acknowledgements

This study was financially supported by the Brazilian governmental agencies FAPESP (2008/03636-5), CNPq and CAPES. The authors thank GPQVA (Grupo de Pesquisa em Química Verde e Ambiental) and Central Analítica of IQUSP for the BET isotherms and the XRD measurements of the catalysts.

Notes and references

[a] Departamento de Química Fundamental, Instituto de Química, Universidade de São Paulo – PO Box 26.077, 05513-970, São Paulo/SP – Brazil

1 T. Ohno, K. Tokieda, S. Higashida, M. Matsumura, *Appl Catal A-Gen*, 2003, **244**, 383.

2 R. Istvn, V. Subramanian, M. Kuno, P. V. Kamat, *J Am Chem Soc*, 2006, **128**, 2385.

3 C.-S. Chou, R.-Y. Yang, C.-K. Yeh, Y.-J. Lin , *Powder Technol*, 2009, **194**, 95.

4 Y.-Z. Zhang, B. Gao, G. L. Puma, A. K. Ray, H. C. Zeng, *Sci Adv Mater*, 2010, **2**, 503.

5 R. Su, R. Tiruvalam, Q. He, N. Dimitratos, L. Kesavan, C. Hammond, J. A. Lopez-Sanchez, R. Bechstein, C. J. Kiely, G. J. Hutching, F. Besenbacher, *ACS Nano*, 2012, **6** 6284.

6 K. Awazu, M. Fujimaki, C. Rockstuhl, J. Tominaga, H. Murakami, Y. Ohki, N. Yoshida, T. Watanabe, *J Am Chem Soc*, 2008, **130**, 1676.

7 M. L. de Souza, P. Corio, *Appl Catal B- Environ*, 2013, **136-137**, 325.

8 K. L. Kelly, E. Coronado, L. L. Zhao, G. C. Shatz, *J Phy Chem B*, 2003, **107**, 668.

9 D. P. Steensma, *Arch Pathol Lab Med*, 2001, **125**, 250.

10 N. Venkatachalam, M. Palanichamy, V. Murugesan, *Mater Chem Phys*, 2007, **104**, 454.

11 B. Wiley, Y. Sun, Y. Xia, *Langmuir*, 2005, **21**, 8077.

12 D. Reyes-Coronado, G. Rodriguez-Gattorno, M. E. Espinosa-Pesqueira, C. Cab., R. de Coss, G. Oskam, *Nanotechnology*, 2008, **19**, 145605.

13 N. Mahdjoub, N. Allen, P. Kelly, V. Vishnyakov, *J Photoch Photobio A*, 2010, **211**, 59.

14 T. Sato, A. Sato, T. Arai, *Colloid Surface A*, 1998, **142**, 117.

15 R. W. Sabnis, in: Taylor & Francis Group (Eds.), *Handbook of Acid-Base Indicators*, 2007, CRC Press., pp. 91.

16 C. Bauer, P. Jacques, A. Kalt, *Chem Phys Lett*, 1999, **307**, 397.

17 E. Pigorsch, A. Elhaddaoui, S. Turrel, *Spectrochim Acta*, 1994, **50**, 2145.

18 C. E. Bonancêa, G. M. do Nascimento, M. L. de Souza, M. L. A. Temperini, P. Corio, *Appl Catal B- Environ*, 2006, **69**, 34.

19 N. Biswas, S. Umapathy, *J Phys Chem A*, 2000, **104**, 2734.

20 D. R. C. Matazo, R. A. Ando, A. C. Borin, P. S. Santos, *J Phys Chem A*, 2008, **112**, 4437.

21 S. C. Li, U. Diebold, *J Am Chem Soc*, 2010, **132**, 64.

22 W. Hou, Z. Liu, P. Pavaskar, W. H., Hung, S. B. Cronin, *J Catal*, 2011, **277**, 149.

